Applied Catalysis B: Environmental 330 (2023) 122662

Contents lists available at ScienceDirect

Applied Catalysis B: Environmental

journal homepage: www.elsevier.com/locate/apcatb

Reaction-driven evolutions of Pt states over Pt-CeO_2 catalysts during CO oxidation

Jinshi Dong [a,*], Yutao Zhang [a], Dekun Li [a], Alexander Adogwa [b], Shijun Huang [a], Ming Yang [b,*], Jiaqiang Yang [c,*], Qianqian Jin [d,*]

[a] Laboratory of New Energy and Environmental Catalysis, School of Biological and Chemical Engineering, Guangxi University of Science and Technology, Liuzhou 545006, Guangxi, China
[b] Department of Chemical and Biomolecular Engineering, Clemson University, Clemson, SC, USA
[c] Zhongyuan critical metals laboratory, Zhengzhou University, Zhengzhou 450001, Henan, China
[d] School of Electronic Engineering, Guangxi University of Science and Technology, Liuzhou 545006, Guangxi, China

ARTICLE INFO

Keywords:
Reaction-driven dynamics
Pt-CeO_2 catalyst
Hysteresis loop
Pt_xO_y ensemble
Initial metal size

ABSTRACT

Pt-CeO_2 catalysts had been comprehensively investigated on the structure-performance relationships in various applications. However, reaction-driven structural dynamics are still in heavily debate. In this study, we tried to track the evolutions of Pt states during CO oxidation. It was found that the activities are not in line with Pt loading amounts; the reactivity started to sharply decrease and the "hysteresis loop" in activity would appear when Pt loading amount is more than 0.25 %. Combining the analyses of chemisorption and spectroscopy technologies, we concluded that Pt single atoms are prone to aggregate into Pt clusters while Pt nanoparticles suffer an oxidation process and gradually form a new Pt species-Pt_xO_y ensembles with the elevated reaction temperatures. Density functional theory calculations further revealed that the different adsorption properties of CO and O_2 on Pt species with different initial sizes are the primary causes of different evolution behaviors.

1. Introduction

Pt-CeO_2 catalysts are widely used in many applications, such as, oxidation [1–7], dehydrogenation [8,9] and hydrogen production from liquid organic carriers [10,11], because of their tunable interactions and charge transfers between the metal and the support. Controlling the exposed facet of CeO_2 to tune the surface structures or adsorbing sites is a common practice of enhancing catalytic reactivity [12–15]. Studies have shown that high-temperature and/or steam treatment can redisperse Pt into a coordination-unsaturated single atom and active CeO_2 surface lattice oxygen thus significantly improving CO oxidation activity [16–20]. In addition, the effect of particle sizes and average oxidation state of metals can substantially influence catalytic reactivity [1,21–23], and it is suggested that moderate reduction treatment to control Pt oxidation states in certain regions could result in the best CO oxidation activities [3,24].

However, the exact structure of metals, especially their oxidation state and dynamics during reactions are still heavily debated [25–27]. Parkinson et al. [28,29] observed CO-induced Pd_1 or Pt_1 sintering on Fe_3O_4 (001) surface through scanning tunneling microscopy (STM). Wang et al. [30] reported an enhancement in CO oxidation performance of Pt_1-CeO_2 after treatment in CO at 275 °C; even part of single-atom Pt species transformed into Pt nanoparticles during this process. A similar phenomenon was also found by Grunwaldt et al. [31,32]. Whereas in CO + O_2 environment, Pt structure and oxidation state dynamics will be much more complex and confused. Seemingly, the changes in Pt states during CO oxidation are closely related to their initial states prior to the reaction; Pt single atoms/sites tend to agglomerate into small clusters while Pt nanoparticles are prone to be partially oxidized [26,27,33,34]. Contrary to the positive viewpoint upon Pt clusters in oxidation reactions, the effects of Pt nanoparticles after being oxidized were difficult to draw a unanimous conclusion [1,34,35]. Some studies indicated that the simultaneous presence of metallic and oxidized metal enables a synergy effect to facilitate CO oxidation and other reactions [1,36–39], while others argued that the formation of platinum oxide during oxidation reaction leads to the deactivation of catalysts [35].

Despite all these efforts, an in-depth understanding of the dynamics of catalysts under reaction conditions is still missing. Addressing this issue requires comprehensive and systematic in situ spectroscopic studies, chemisorption, and kinetics analyses, and density functional

* Corresponding authors.
E-mail addresses: jinshidong@gxust.edu.cn (J. Dong), myang3@clemson.edu (M. Yang), jqyang@zzu.edu.cn (J. Yang), qqjin10s@139.com (Q. Jin).

https://doi.org/10.1016/j.apcatb.2023.122662
Received 1 March 2023; Accepted 17 March 2023
Available online 20 March 2023

theory (DFT) calculations. By using these approaches, herein, we conduct a detailed investigation of the dynamic changes of Pt supported on CeO_2 with different loadings. Through tracking the structure and oxidation state evolutions of Pt species and timely linking the above information with the transient activities during CO oxidation, it is concluded that Pt single atoms will aggregate into Pt small clusters containing a few platinum atoms to keep a high activity, in contrast, Pt nanoparticles (~1.1 nm) are prone to be gradually oxidized into Pt_xO_y ensembles which suffer from a significant loss in activity according to the degree of oxidation.

2. Experimental

2.1. Synthesis of Pt-CeO_2 catalysts

CeO_2 support was synthesized by heating $Ce(NO_3)_3{\cdot}6\ H_2O$ (99.5 %, Macklin) in flowing air at 350 °C for 2 h and then at 500 °C for 3 h. Pt (precursor: $H_2PtCl_6{\cdot}6\ H_2O$, aladdin) was loaded on CeO_2 samples by incipient wetness impregnation (IWI) method, the loading amounts of Pt are respectively 0.05 %, 0.1 %, 0.25 %, 0.5 % and 0.75 % (weight fractions). The samples were then dried under infrared lamp prior to calcination at 400 °C for 4 h in muffle furnace to get the catalysts with different Pt loading amounts and denoted as 0.05–0.75Pt-CeO_2.

2.2. Catalyst characterization

CO adsorption diffuse reflectance infrared Fourier transform spectroscopy (CO-DRIFTS) were performed on a Nicolet iS50 FTIR spectrometer equipped with Pike high temperature reaction chamber using a ZnSe window. In a typical ex-situ measurement, ~20 mg catalyst was placed in the sample storehouse with quartz wool filled the bottom and the metal net was paved under the quartz wool to prevent the blocking of gas outlet. The upper surface of the catalyst power was then troweled and afterwards 200 ml/min Ar (99.999 %) flowed downwards through the sample for 10 min to remove air in the system. For the CO-DRIFTS experiments of the reduced catalysts, the sample was first reduced in 5 % H_2/Ar (100 ml/min) at 300 °C for 15 min. After cooling to room temperature (RT), Ar flow purged for 10 min and a spectrum was then recorded as background. Subsequently, a gas flow of 10 % CO/Ar (50 ml/min) was introduced into the reaction cell for 10 min and the inlet flow was switched to Ar (200 ml/min) and kept for 60 s, after which the spectrum was recorded. In a typical in situ reaction measurement, the operations were the same as the above procedures, except after the reduction and cooling to RT step, the reaction feeds purged, and the sample was heated to a targeted temperature at the rate 15 °C/min and kept for 60 s before cooling. For the catalysts treated at a temperature low than 165 °C, Ar was directly switched during the cooling processes, while for the catalysts treated at a high temperature as more than 300 °C, the reaction feeds would be kept during the cooling step until the temperature reached ~150 °C then Ar was switched to avoid Pt sintering in Ar at a high temperature. The reaction feeds denoted as CO+O_2, CO and O_2 atmospheres consist of 1 % CO + 2 % O_2 balanced with Ar, 1 % CO balanced with Ar and 2 % O_2 balanced with Ar, respectively. The total flow rates are all 200 ml/min for these three groups.

Transmission electron microscopy (TEM) studies were conducted on an aberration corrected JEM-ARM 200F (JEOL) field emission electron microscope. The high-angle angular dark-field scanning transmission electron microscopy (HAADF-STEM) images were collected by an annular dark-field detector in the range of 54–220 mrad with a convergence angle of 20.6 mrad. The testing samples were prepared by dropping the ethanol-diluted catalyst suspension on TEM grids coated with holey carbon film.

The temperature programmed reduction by hydrogen (H_2-TPR) experiments were conducted on a homemade Builder PCA-1200 chemisorption analyzer. In a typical H_2-TPR experiment, 50 mg catalyst mixed with 0.75 g quartz sand was put between the upper and lower quartz wool in the U-shaped quartz tube. Prior to the H_2-TPR experiments the catalysts were pretreated at 200 °C in Ar (200 ml/min) for 30 min and cooled down to room temperature. 10 % H_2/Ar was then switched with a flow rate of 30 ml/min for both testing and reference gas channels. Afterwards the thermal conductivity detector (TCD) was turned on and its temperature was controlled at 80 °C, after the base line reached smooth and steady the sample was heated with a heating rate of 10 °C/min from RT to 600 °C to get the H_2-TPR profile. The drying agent cell fixed in gas line between the testing sample and TCD was immersed in ice-water bath during the whole experiment to eliminate the peak of water in the H_2-TPR profile.

X-ray photoelectron spectroscopy (XPS) experiments were conducted on a Thermo fisher Scientific K-Alpha spectrometer using a monochromatic Al Kα (1486.6 eV) X-ray excitation source operated at 12 kV. All the catalyst samples were rapidly transferred to vacuum tubes in glove box filled with Ar and kept in the designed atmosphere conditions, before XPS tests. The samples were also loaded on the holder in the glove box to avoid the changes of Pt states. For the catalysts treated at a temperature low than 165 °C, Ar was directly switched during the cooling process, while for the catalysts treated at a high temperature as more than 300 °C, the reaction feeds would be kept during the cooling step until the temperature reached ~150 °C then Ar was switched to avoid Pt sintering in Ar at a high temperature. After the measurements, the binding energies were calibrated using the C 1 *s* line at 284.8 eV as reference.

The amount of Pt loadings were measured by inductively coupled plasma (ICP) on a Agilent 7700 spectrometer. BET surface area analyses were conducted on a Micromeritics ASAP 2460 physical adsorption apparatus. Prior to the measurements, the samples were degassed at 200 °C under vacuum for 4 h.

2.3. Catalytic activity and kinetics measurements

In a typical CO oxidation reaction test, 50 mg catalyst diluted with 0.75 g quartz sand was placed between the quartz wool in a U-type quartz tube reactor. The CO oxidation light-off tests were conducted at a heating rate of 15 °C/min. The feed gas consisted of 1 % CO, 2 % O_2 balanced with Ar at a total flow rate of 500 ml/min. CO, O_2 and CO_2 concentrations were monitored by an HPR-20 R&D online mass spectrometer (Hiden Co. Ltd). Before testing, the initial gas concentrations would be calibrated using the quantitative analysis software called "QGA professional" according to the accurate flow rate of every gas determined by mass flowmeters. For the tests of reduced samples, the catalysts were first reduced at 300 °C in 5 % H_2/Ar at a flow rate of 100 ml/min for 15 min before tests. The kinetic measurements of the CO oxidation reaction were performed under the condition that CO conversion was below 20 % to eliminate the thermal and diffusion effects.

2.4. Computational details

Density functional theory (DFT) calculations [40] were carried out using plane waves as implemented in Vienna Ab initio Simulation Package (VASP) [41–44]. The exchange and correlation energy was treated by generalized gradient approximation (GGA) with the Perdew–Burke–Ernzerhof (PBE) [45] form generated using the projector augmented wave (PAW) method [46]. The DFT+U method was implemented to diminish the self-interaction error and the Hubbard term U was set as 5.0 eV for the Ce 4 *f* states [47,48]. The Kohn-Sham single electron orbitals were expanded by plane waves with an energy cutoff of 400 eV. The geometry optimization was converged when the maximum force on each atom was less than 0.05 eV/Å.

The 2 × 4 c(2 ×2) CeO_2 (1 1 1) surface with six atomic layers (two trilayers) were cleaved from cubic CeO_2 unit cell. A vacuum layer of 15 Å in the z direction (perpendicular to the surface plane) was used to separate the surface slab and a Monkhorst–Pack grid size 2 × 2 × 1 was used to sample the surface Brilliouin zone for these three surface slabs.

All atoms of the adsorbate layer and the top three CeO_2 atomic layers (one tri-layers) were allowed to relax while other atoms in the surface slab were fixed during the optimization. Adsorption energies were determined as $E_{adsorption} = E_{adsorbate\ /surface} - E_{adsorbate} - E_{surface}$, where $E_{adsorbate\ /surface}$ is the calculated energy of the adsorbate on CeO_2 system, $E_{adsorbate}$ is the energy of the adsorbed molecule (such as CO and O_2) in crystal box and $E_{surface}$ is the energy of CeO_2 surface created above. The detail calculations of forming energy were shown in Supplementary Note 3 and 4. Bader charge analyses were implemented with a fast algorithm developed by Henkelman et al. [49]. The stretching frequencies of CO were calculated within the harmonic approximation, and all atoms are fixed except CO and its first neighboring atoms during the relaxations [50,51].

3. Results and discussion

3.1. CO oxidation activities of Pt-CeO_2 catalysts and their initial structures

A series of Pt-CeO_2 catalysts with Pt loadings from 0.05 to 0.75 wt% were synthesized by the method of incipient wetness impregnation and the calcination temperature was 400 °C. Through testing, reduction pretreatments could substantially improve the activities of these catalysts (Figs. S1a and 1b) and the best reducing temperatures in 5 % H_2/Ar were 300 °C for most catalysts (data not shown). Fig. 1a showed the light-off profiles of Pt-CeO_2 catalysts after 300 °C reductions. It was found 0.1Pt-CeO_2-300H displayed the best reactivity in CO oxidation. Whereas when Pt loading is more than 0.25 wt%, the catalytic activity sharply decreased and an interesting "hysteresis loop" was observed upon the light-off curve; when the temperature increased more than ~130 °C, CO conversion decreased until the temperature reached ~290 °C, after that the light-off curve increased again (Fig. 1a). To illustrate this phenomenon, 0.1–0.5Pt-Al_2O_3 catalysts were fabricated by the same procedure and the light-off profiles of the reduced samples are shown in Fig. 1b, hysteresis curves were rather absent for these Pt-Al_2O_3 catalysts. Thus, it is concluded that the hysteresis effect in activity is closely related to the loading amount of metal and the support used.

Because of the redox property of CeO_2, we speculate that the deactivation of Pt-CeO_2 during CO oxidation is due to the oxidation of Pt species [35]. However, this oxidized Pt species is different from the Pt species before reduction (Fig. 1c). The apparent activation energy (E_a) results further verified that Pt sites are almost the same despite the loading amounts for the reduced Pt-CeO_2 catalysts (before activity hysteresis), or the reduced Pt-Al_2O_3 catalysts, or Pt-CeO_2 catalysts before reductions (Fig. 1d-f, Figs. S1c and 1d). The E_a value of the reaction-driven oxidized Pt species on CeO_2 is a little more than that of the reduced Pt but far less than that of the unreduced Pt species (Figs. 1d and 1 f), indicating that the oxidation of Pt during CO oxidation is a facile change in chemical structure instead of transformation into crystal Pt oxide. In addition, the exposed facet of CeO_2 support was also proved to be a key factor affecting the performance of Pt-CeO_2 catalyst. The CeO_2 materials with different exposed facets were synthesized by hydrothermal methods in our previous work [14], and the materials' general information was summarized in Table S1. As a result, the reduced 0.5Pt-CeO_2 (111) and (110) catalysts displayed hysteresis in activity while the reduced 0.5Pt-CeO_2 (100) catalysts did not (Fig. S2a). According to our previous analyses, CeO_2 (100) surface oxygen is easy to be removed during the reduction process to form a Ce-terminated surface. In contrast, higher oxygen vacancy (O_v) formation energies on (111) and (110) surfaces cause lots of surface lattice oxygen around Pt species [14]. The interfacial Pt-O-Ce bonds contribute to the catalytically-driven oxygen transfer [52], and even increasing the reduction temperature to 350 °C, the hysteresis phenomenon still exists (Fig. S2b). However, Pt-CeO_2 catalyst after high temperature (such as

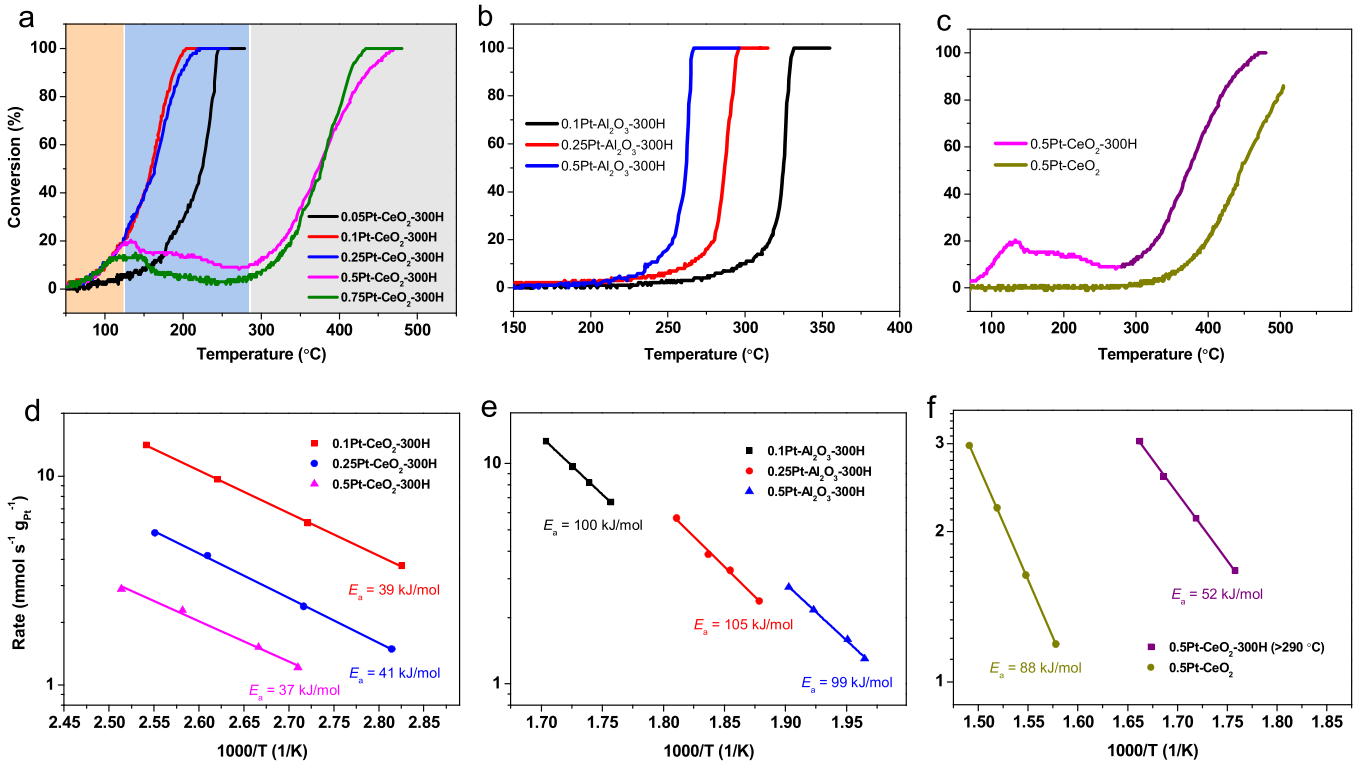

Fig. 1. CO oxidation activities and apparent kinetics analyses of Pt-CeO_2 and Pt-Al_2O_3 catalysts. CO oxidation light-off profiles of (a) Pt-CeO_2 catalysts after H_2 reductions, (b) Pt-Al_2O_3 catalysts after H_2 reductions and (c) 0.5Pt-CeO_2 catalysts before and after H_2 reduction. Arrhenius plots of (d) Pt-CeO_2 catalysts after H_2 reductions, (e) Pt-Al_2O_3 catalysts after H_2 reductions and (f) 0.5Pt-CeO_2 catalysts before H_2 reduction and after H_2 reduction more than 290 °C. Feed gas stream: 1 % CO and 2 % O_2 balanced with Ar, flow rate: 500 ml/min. 50 mg catalyst was used for each sample. These series of Pt-CeO_2 and Pt-Al_2O_3 catalysts were obtained by calcination at 400 °C. The reduction treatments were conducted at 300 °C in 5 % H_2/Ar (denoted as X-300H).

800 °C) calcination seems no hysteresis observed in activity because of the redispersion of Pt on CeO_2 by atom trapping [30].

Pt single atoms (Pt_1) are the dominating species both in the reduced 0.05 and 0.1Pt-CeO_2 catalysts, while Pt nanoparticles (Pt^0) are the main Pt species when Pt loading is more than 0.25 wt%, as illustrated by the CO-DRIFT spectra (Fig. 2a). The TEM images further visually affirmed that Pt single atoms and Pt clusters (composed by several atoms) co-exist in 0.1Pt-CeO_2-300H sample, and in 0.25Pt-CeO_2-300H Pt single atom, Pt cluster and Pt nanoparticle morphologies all could be found, whereas Pt nanoparticles with the mean size of 1.1 nm mainly exist in 0.5Pt-CeO_2-300H among these morphologies (Fig. 2d-f). Pt surface concentrations (in μmol m^{-2}) of various Pt-CeO_2 catalysts were calculated by Pt loading amount (measured by ICP) dividing surface area of each catalyst after reduction, the results are shown in Table S2. It can be concluded that when Pt surface concentration is more than 0.04 μmol m^{-2} Pt cluster would appear, while Pt nanoparticle would become the dominating morphology when the value is more than 0.20 μmol m^{-2}. Notably, the CO adsorbing signals disappeared at room temperature for these Pt-CeO_2 catalysts without reduction treatments except 0.75Pt-CeO_2 (Fig. 2b), indicating Pt oxides are the dominating Pt species before reductions [53], only a small amount of Pt cluster could be found in a higher Pt loading (0.75 wt%) sample (Fig. 2b). In contrast, the reduced Pt-Al_2O_3 catalysts exhibited identical Pt nanoparticle morphologies regardless of Pt loading amounts (Fig. 2c), though before reductions they are all Pt oxides as in Pt-CeO_2 catalysts (Fig. S3). The TEM images further verified the mean sizes of Pt nanoparticles are 1.4–1.7 nm for 0.1–0.5Pt-Al_2O_3-300H samples (Fig. S4), which were much larger than corresponding Pt-CeO_2 catalysts. Accordingly, the surface nature of support significantly affects the size of metal and the catalytic reactivity.

3.2. The evolutions of Pt-CeO_2 catalysts during CO oxidation

Fig. 3a and b showed the H_2-TPR profiles of Pt-CeO_2 catalysts before H_2 reductions and the reduced Pt-CeO_2 catalysts after 200 °C CO oxidation reactions, respectively. The H_2 consumption around 350–550 °C is attributed to surface oxygen on ceria [56], as verified by the H_2-TPR profiles of bare ceria materials (Fig. S5). The peak ranging from 250 °C to 350 °C is assigned to the reduction of Pt oxide for the samples of 0.25–0.75Pt-CeO_2 according to our previous study [14]. However, this reduction peak of Pt oxide was absent in 0.05 and 0.1Pt-CeO_2 samples, instead they both exhibited a reduction peak centered at 88 °C and subsequent shoulder peak below 250 °C (Fig. 3a), and coincidentally, these low-temperature reduction peaks were not found in 0.25–0.75Pt-CeO_2 samples even in the enlarged profiles (Fig. S6). Combining the analyses of CO-DRIFTS (Fig. 2a) above, the reduction peak centered at 88 °C and subsequent shoulder peak in H_2-TPR profiles are doubtless the reduction peaks of the oxidized precursor species of Pt single atoms and simultaneous migration process on CeO_2 surface [21,24,57]. The oxidized Pt single atoms are mainly distributed at the step sites or at substituted Ce sites of CeO_2 surface [18,57,58]. For the reduced 0.05–0.25Pt-CeO_2 catalysts after 200 °C CO oxidations, the consistent reduction peaks centered at ~149 °C (Fig. 3b) were attributed to the reduction of oxygen close to the Pt-ceria interface [56], which was produced during CO oxidation. Noteworthily, the aggregation states of Pt kept almost the same after CO oxidation for the reduced 0.05–0.25Pt-CeO_2 catalysts, despite of the difference before reaction. Fig. 3c further verified for the low-loading samples the newly formed Pt states during reactions are Pt clusters whether at 120 °C (~T_{20} temperature) or 160 °C (~T_{50} temperature). However, for the high-loading samples after CO oxidation, the reduction peak with a

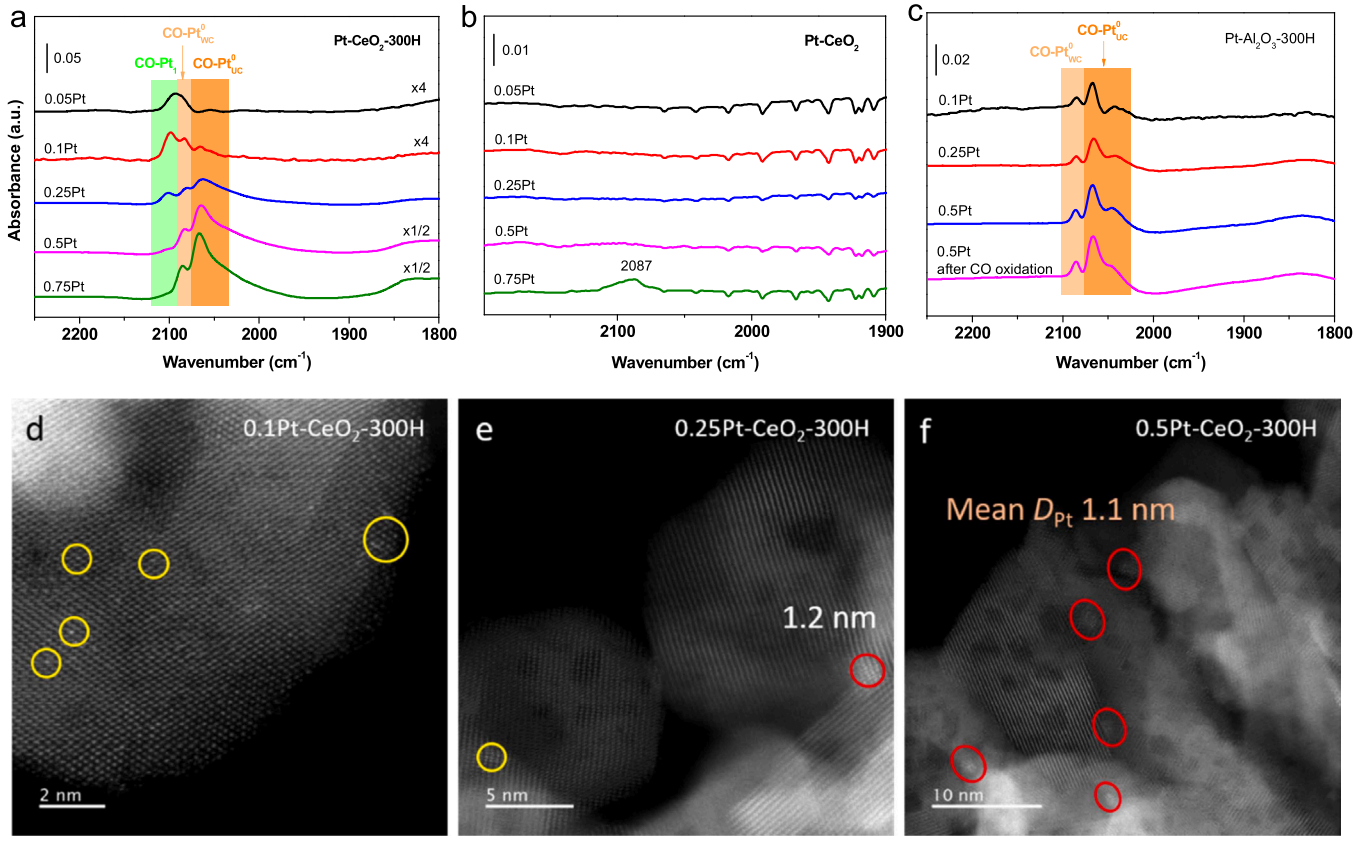

Fig. 2. The initial states of Pt on CeO_2 or Al_2O_3 with different loadings. a-c, Room temperature CO-DRIFT spectra of (a) Pt-CeO_2 catalysts after H_2 reductions, (b) Pt-CeO_2 catalysts before H_2 reductions and (c) Pt-Al_2O_3 catalysts after H_2 reductions. TEM images of reduced Pt-CeO_2 catalysts with Pt loadings of (d) 0.1 wt%, (e) 0.25 wt% and (f) 0.5 wt%. Pt^0_{WC} and Pt^0_{UC} are respectively assigned to CO linearly adsorbed on well-coordinated Pt sites and under-coordinated Pt sites of Pt nanoparticles [54,55].

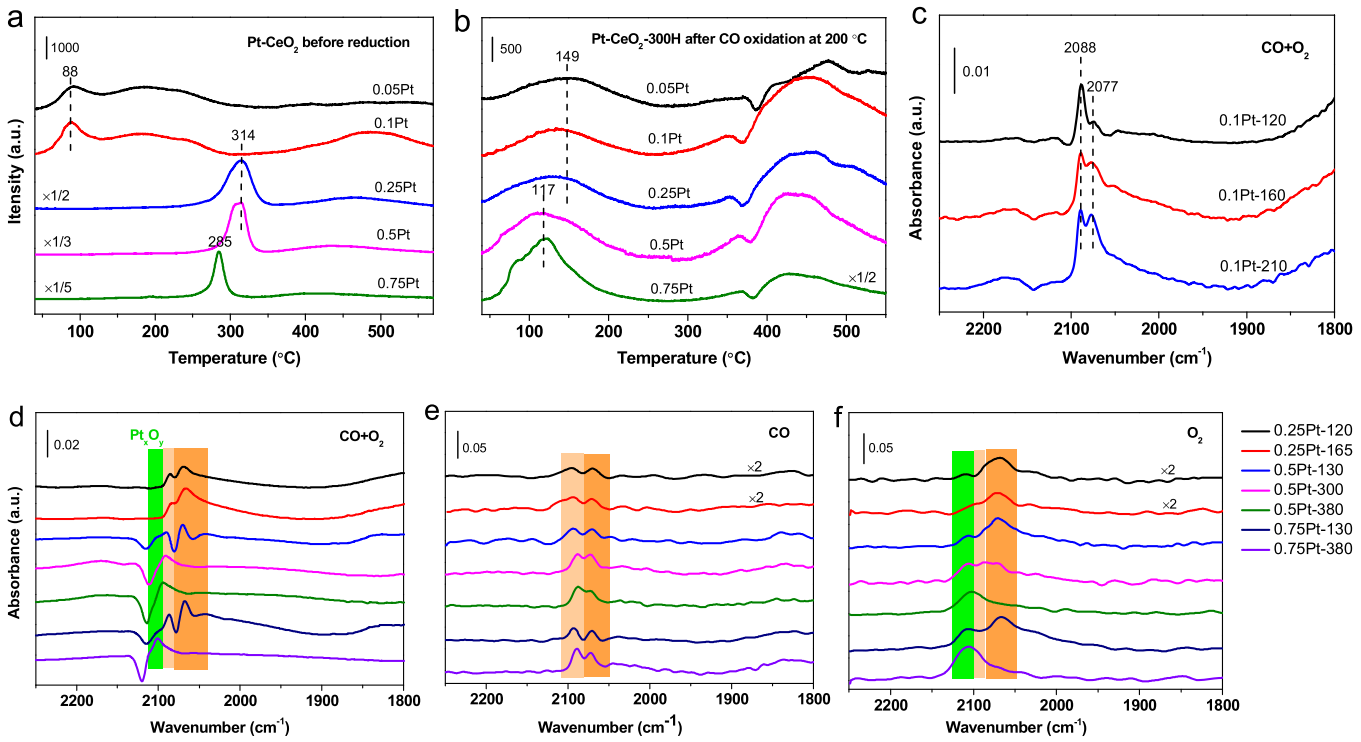

Fig. 3. The dynamic structures of Pt under different atmospheres. H_2-TPR profiles of Pt-CeO_2 catalysts (a) before H_2 reductions and (b) the reduced Pt-CeO_2 catalysts after 200 °C CO oxidation reactions. (c) In situ CO-DRIFT spectra of the reduced 0.1Pt-CeO_2 catalyst after being exposed in CO and O_2 gases at 120 °C and 160 °C for 1 min (denoted as 0.1Pt-120 and 0.1Pt-160, respectively, and similarly hereinafter). In situ CO-DRIFT spectra of the reduced 0.25–0.75Pt-CeO_2 catalysts after being exposed in (d) CO and O_2 reaction gases, (e) CO and (f) O_2 at different temperatures. The heating rate, feed concentrations and gas hourly space velocity (GHSV) of in situ CO-DRIFT experiments were the same as CO oxidation activity tests. Every infrared spectrum was collected after collecting its own individual background at ambient temperature, and Ar would purge for 60 s prior to collect the spectrum each time.

lower temperature centered at ~117 °C was appeared (Fig. 3b), which was among the reduction temperatures of the oxidized precursor of Pt single atom (88 °C) and in situ formed Pt clusters (149 °C), another feature is the H_2 consumption amounts were obviously more than those of the low-loading samples. Accordingly, we deduced that the reduction peaks centered at ~117 °C were assigned to the in situ formed oxidized Pt clusters/nanoparticles or called Pt_xO_y ensembles. More about the H_2-TPR analyses can be seen in Supplementary Note 2.

Comparing the CO-DRIFTS of the reduced 0.1Pt-CeO_2 before and after CO oxidation (Fig. 2a and Fig. 3c), it is concluded that low-coordinated Pt single atoms formed by H_2 reduction are prone to aggregate into Pt clusters during heating oxidation reaction, which is in well consistent with previous reports [8,22,34]. Besides, the sizes of Pt clusters increased with the increasing reaction temperature (Fig. 3c). Fig. 3d-f showed the in situ CO-DRIFTS of the reduced 0.25–0.75Pt-CeO_2 catalysts after being exposed in CO+O_2 atmosphere or single CO or single O_2 at the temperatures of ~20 % or ~50 % CO conversions in the light-off profiles. The CO adsorbing signal at around 2100 cm^{-1} can be assigned to CO on the Pt sites of Pt_xO_y ensembles apart from on Pt single atoms [21,55]. According to the above analyses, Pt single atoms would sinter into Pt clusters during CO oxidation. Thus, the peaks around 2100 cm^{-1} in Figs. 3d and 3 f are attributed to CO adsorbing on Pt_xO_y ensembles. It can be found that only a bit of Pt_xO_y ensembles formed at the temperature low than 130 °C during CO oxidation for the samples with Pt loading more than 0.25 %, while when the temperature reached 300 °C, Pt species totally transformed into Pt_xO_y ensembles (Fig. 3d). However, the reduced catalysts with lots of Pt single atoms and clusters (such as the reduced 0.25Pt-CeO_2 sample) were difficult to be oxidized, even at the temperature as high as 300 °C (Fig. 3d and Fig. S7).

Under single O_2 atmosphere, Pt species are likewise easy to be oxidized as those under CO+O_2 atmosphere at the same temperatures (Figs. 3d and 3 f). Whereas all the Pt species would sinter into bigger clusters/nanoparticles under single CO atmosphere for the reduced 0.25–0.75Pt-CeO_2 catalysts at all conditions (Fig. 3e), suggesting the reduction effect of CO gas as previous reports [26,28–32]. It should be noted that the negative peaks appeared at ~2118 cm^{-1} in the CO-DRIFTS of the catalysts after CO oxidation (Fig. 3d), may be attributed to the changes of CeO_2 surface Ce^{3+} sites involved in the CO oxidation reaction [59]; specifically, the O_v (as well as Ce^{3+}) sites were formed after reduction pretreatments, and during CO oxidation the O_v would be filled by O_2 to react with CO, thus Ce^{3+} would transformed to Ce^{4+} in this process, resulting in the negative peaks in the CO-DRIFTS spectra. Accordingly, CO and O_2 play different roles in the evolutions of Pt species during CO oxidation; CO makes Pt species to be reduced and sintered while O_2 makes them oxidized and anti-sintered. As a result, Pt single atoms are more prone to be affected by CO while O_2 affects Pt nanoparticles more strongly during CO oxidation. It is worth stressing that the existing of gas-phase spectrum of CO will make it very complex to analyze chemisorbed CO on Pt and PtO_x species [60,61], here Ar would purge for 60 s prior to collect the spectrum each time to eliminate the signal of gas-phase CO, as conducted by other studies [14,18,62]. Of course, this method will neglect some information of adsorbed CO and its reactivity [63]. However, CO-DRIFTS in this research are mainly used to illustrate the evolution of Pt species, thus it will not affect the analysis results.

The Pt species are dominating PtO crystals with the sizes in several nanometers for 0.5Pt-CeO_2 sample before reduction (Figs. 4a and 4c). After reduction treatment, this sample showed mean size of 1.1 nm Pt nanoparticles with 50.2 % metal state (Fig. 2f and Fig. 4 f), while after CO oxidation at 300 °C, the ratio of Pt metal state (Pt^0) further decreased to 35.1 % and the sizes of Pt species increased a bit more than 1.1 nm (Fig. 4b and Fig. 4c), combing the analyses of H_2-TPR profiles (Figs. 3a and 3b) and the activity difference between this in situ formed Pt species and oxidized Pt_1 (Fig. 1c and Fig. S1a), we suggest Pt_xO_y species instead

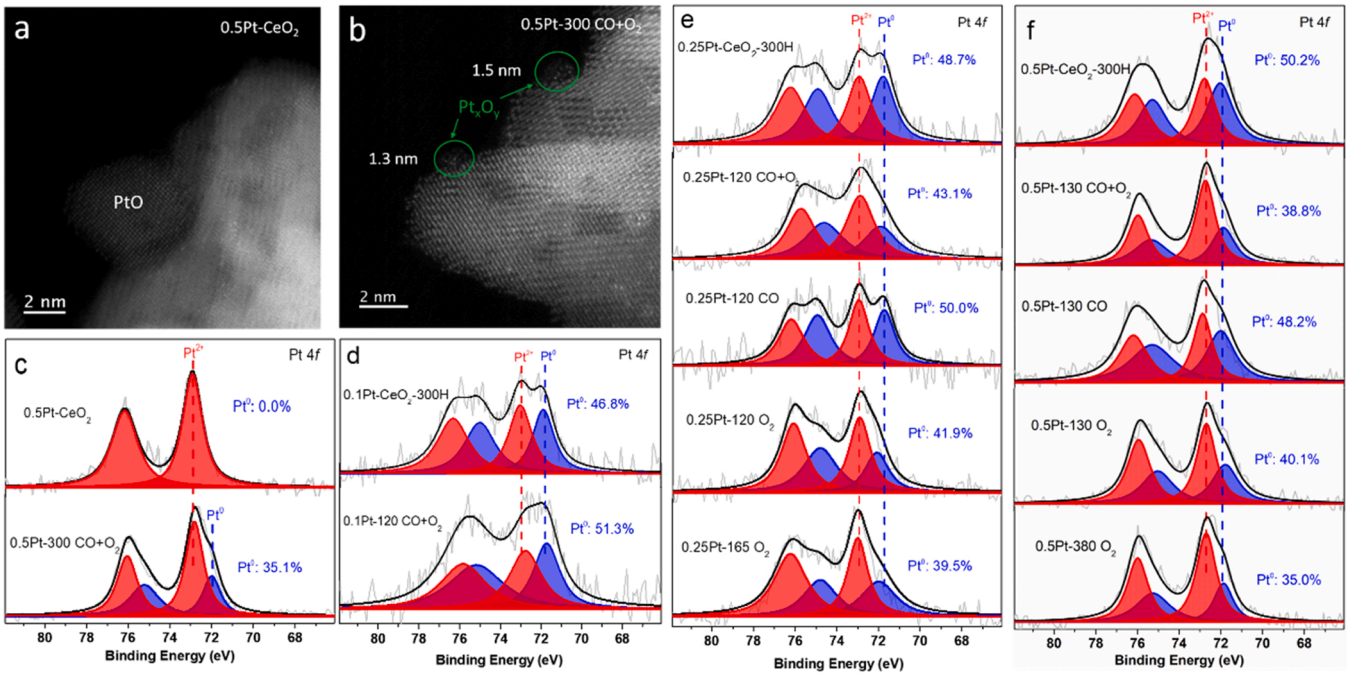

Fig. 4. Reaction-induced changes of Pt chemical states. TEM images of (a) as prepared 0.5Pt-CeO_2 catalyst and (b) the reduced 0.5Pt-CeO_2 catalyst after 300 °C CO oxidation. XPS spectra of (c) 0.5Pt-CeO_2 catalysts before and the reduced sample after 300 °C CO oxidation, (d) the reduced 0.1Pt-CeO_2 catalysts before and after 120 °C CO oxidation, (e) the reduced 0.25Pt-CeO_2 catalysts under different atmospheres and (f) the reduced 0.5Pt-CeO_2 catalysts under different atmospheres. All the catalyst samples were rapidly transferred to vacuum tubes in glove box filled with Ar after being kept in the designed conditions. Before XPS tests, the samples were also loaded on the holder in the glove box to avoid the changes of Pt states. Pt^{4+} was difficult to deconvolve in the above XPS Pt 4 *f* spectra, thus only Pt^{2+} and Pt^0 were deconvolved, as conducted by other reports [30,65].

of Pt single atoms were mainly formed for the reduced 0.5Pt-CeO_2 catalyst after CO oxidation at 300 °C.

For the sample 0.1Pt-CeO_2-300H after CO oxidation at 120 °C, Pt^0 ratio surprisingly increased, verifying the sintering of Pt species during CO oxidation, which in well consistence with the CO-DRIFTS shown in Fig. 3c. In contrast, for the reduced 0.25Pt and 0.5Pt-CeO_2 after CO oxidation at 120 °C or 130 °C, Pt^0 ratios were inversely decreased (Figs. 4e and 4 f), illustrating the oxidation of Pt species during the reaction. It should be noted that the hysteresis in activity was absent for the reduced 0.25Pt-CeO_2 sample even Pt species were partly oxidized during CO oxidation, presumably because of the existence of abundant Pt single atoms and clusters before reaction (Fig. 2a), their positive performance balanced the deactivation of oxidized Pt species. That is the reason why the light-off activity of the reduced 0.25Pt-CeO_2 was almost the same as the reduced 0.1Pt-CeO_2 (Fig. 1a). In addition, Pt_xO_y species are not active for CO oxidation until the temperature reached 290 °C in our case, which is in line with the conclusion of Christopher et al. that Pt_{ox} was essentially inactive for oxidation of CO below ~200 °C [55]. However, this in situ formed Pt_xO_y species under reaction condition may be different from PtO_2 species created by certain atmosphere which is a highly reactive species that will react with Pt°-CO to give CO_2, as stressed by Meunier et al. [1,63]. It needs to be emphasized that the performance of oxidized metal cluster may differ due to the nature of metals and their surrounding chemical environment; such as, oxidized Pd cluster (Pd_8O_x) on CeO_2 was verified to perform better than metallic Pd cluster (Pd_8) in CO oxidation [64].

Of course, the reduction or sintering effect of CO and the oxidation effect of O_2 were further substantially confirmed by Pt chemical states, and with the increasing temperature of oxidation atmosphere, the degree of oxidation of Pt species was increased accordingly (Figs. 4e and 4 f), these results were also in line with corresponding CO-DRIFTS analyses above. The Pt 4 *f* XPS further manifested that the evolutions of Pt states during CO oxidation were loading dependent or said initial state dependent.

Because of Pt state evolution during CO oxidation with the increasing temperature, the active site will be different from its initial state, here we calculated the reaction rates (in μmol g_{Pt}^{-1} s^{-1}) at different temperatures of 0.5Pt-CeO_2-300H, as well as those of other Pt-CeO_2 catalysts in recent literature and the results are summarized in Table S3. It can be found the reaction rates of Pt-CeO_2 catalysts with different Pt states displayed wide gaps. In our case, the in situ formed Pt_xO_y species at the temperature as high as 300 °C can reach similar reaction rate of Pt nanoparticle at 100 °C. In comparison, partially oxidized Pt nanoparticles (PtO_x) on CeO_2 which were created by a series of treatments of CO and O_2 showed the rate of about 160 μmol g_{Pt}^{-1} s^{-1} even at room temperature [1], while Kopelent et al. [66] demonstrated a reaction rate of ~67 μmol g_{Pt}^{-1} s^{-1} when ceria lattice oxygen was involved in CO oxidation of Pt nanoparticle (Table S3), Meunier et al. [63] further verified CO adsorbed on reduced Pt site could react with oxygen from the redox support or from an adjacent oxidized Pt phase at room temperature. Wang et al. [21] even stated that Pt atom in the ensemble is 100–1000 times more active than its single-atom Pt_1/CeO_2 parent in catalyzing the low-temperature CO oxidation.

3.3. DFT calculation studies

During the H_2 reduction process, oxygen vacancy (O_v) formed through the reaction $H_2 + O \rightarrow H_2O$. O 1 *s* XPS spectra of the reduced 0.1–0.5 Pt-CeO_2 catalysts were shown in Fig. S8a-c. It can be found the amount of oxygen vacancy increased with increase in Pt loading amount or said Pt size. This phenomenon was also observed by Libuda et al. [67] and Kwak et al. [68]. To elucidate this issue, DFT calculations were conducted and firstly we used Pt_1, Pt_4 and Pt_{10}-CeO_2 (111) structures (Fig. 5b-d) to simulate the experimental Pt single atom, Pt cluster and Pt nanoparticle with mean size of ~1.1 nm on CeO_2 surface, respectively, according to the previous reports [21,50,51]. Fig. S9–S12 showed the relaxed structures of Pt_1, Pt_4 and Pt_{10}-CeO_2 (111) with O_v and corresponding forming energies of oxygen vacancy at 300 °C (the H_2

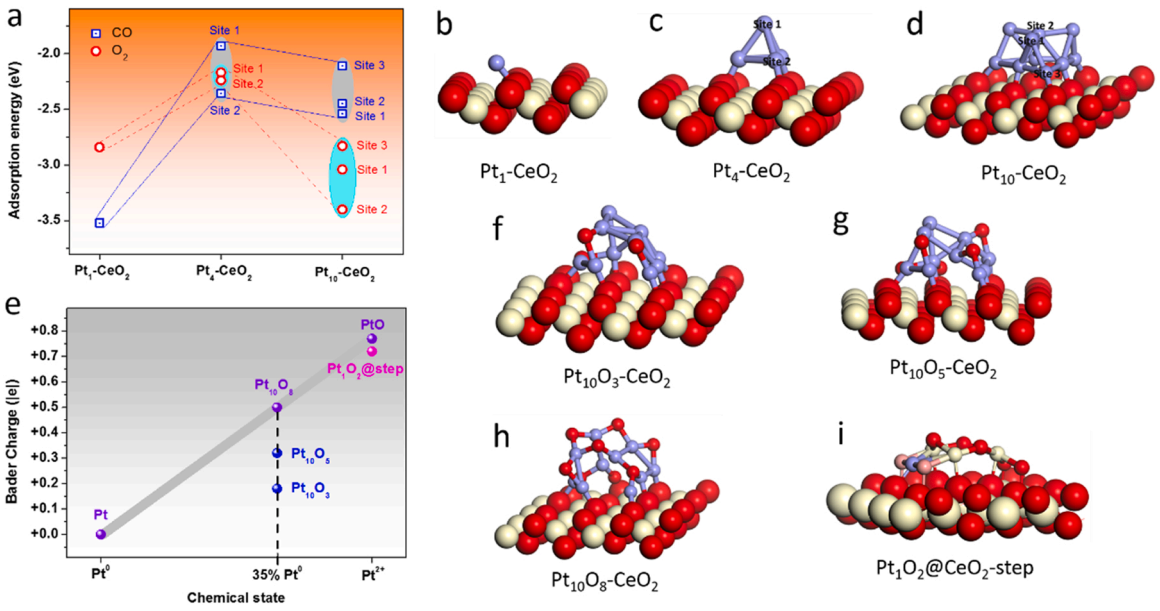

Fig. 5. The formation of Pt_xO_y ensemble and its representative structure. (a) The adsorption energies of CO and O_2 on Pt-CeO_2 catalysts with different Pt sizes. The relaxed structures of (b) Pt single atom Pt_1-CeO_2, (c) Pt cluster Pt_4-CeO_2 and (d) Pt nanoparticle Pt_{10}-CeO_2, different adsorption sites on Pt were marked. (e) The calculated Bader charges of Pt in different coordinated environments vs corresponding chemical states experimentally. The relaxed structures of (f) $Pt_{10}O_3$-CeO_2, (g) $Pt_{10}O_5$-CeO_2, (h) $Pt_{10}O_8$-CeO_2 and (i) Pt_1O_2 @CeO_2-step. The non-defected Pt-CeO_2 models shown above were clarified the surface structures with O_v being filled during CO oxidation. Color: Ce, yellow; lattice O, red; O in Pt_1O_2, pink; Pt, purple.

reduction temperature in experiment). It was concluded that 1) O_v tends to form at the CeO_2 surface site that bonds to Pt species, 2) O_v forming energy decreases with the increase of Pt size and it is thermally preferred at 300 °C when Pt size is large than Pt_4 cluster, 3) two O_vs at the surface oxygen sites bonded to Pt_{10} species can be formed at 300 °C in thermodynamics, but should at the para-oxygen sites (Fig. S12).

Oxygen vacancies play vital important roles in both the adsorption of gaseous O_2 and migration of the bulk lattice oxygen to the surface, and surface oxygen vacancies could provide coordinatively unsaturated sites to induce strong interactions with molecular O_2 [48,52,69]. Our calculation results revealed the adsorption energies of O_2 on the Pt sites next to O_v were much lower than those of O_2 on other Pt sites both for Pt_4 and Pt_{10}-CeO_2 samples, moreover, the Pt site next to O_v is preferred to be adsorbed by molecular O_2 rather CO (Fig. S13 and 14). Two molecular O_2 respectively adsorbing on two Pt sites next to para-oxygen vacancies of Pt_{10}-CeO_2 is also of thermodynamic feasibility (Fig. S14d). The proposed CO oxidation mechanisms on Pt_4 and Pt_{10}-CeO_2 with O_2 pre-adsorbing on interfacial Pt sites next O_v were shown in Fig. S16 and 17. The calculated energy barriers are almost the same for CO oxidation on Pt_4 and Pt_{10}-CeO_2 (1.04 eV and 1.00 eV, respectively), which in well consistent with the experimental results shown in Fig. 1d. After initial reaction, the O_v sites would be filled by adsorbed O atom, of course, O_v would appeared again with the continued CO oxidation through the path of CO reacting with O close to the Pt perimeter sites. It is a dynamic process during reaction, but the amounts of O_v would indeed be reduced when the reaction is finished, as illustrated in Fig. S8. Thus, the following research will focus on the non-defected Pt-CeO_2 catalysts.

Fig. 5a showed the distribution map of adsorption energies of CO and O_2 on different Pt sites of Pt_1, Pt_4 and Pt_{10}-CeO_2 (111), respectively. The different adsorbing Pt sites are marked in Fig. 5b-d (equivalent sites were not labelled), and the relaxed structures after adsorptions are shown in Fig. S18-S20. It can be found that the adsorption energy of CO is much lower than that of O_2 on Pt_1-CeO_2, illustrating a stronger adsorption for CO on Pt single atom. While the adsorption energies of CO and O_2 on Pt_4-CeO_2 both increase and share similar mean values for these two adsorbates (Fig. 5a). Surprisingly, when Pt size increases to Pt_{10} scale, the adsorption energies of CO and O_2 inversely decrease and the adsorption energies of O_2 on all equivalent Pt sites are considerably lower than those of CO on the same Pt sites. These results strongly suggest that O_2 is much easier to adsorb on Pt sites of nanoparticle-sized Pt-CeO_2 catalyst, as reported by Stair et al. [70] based on spectroscopic experiments. The strong chemistry between O_2 and Pt nanoparticle is the right origin of the formation of Pt_xO_y ensemble.

Bader charge calculations were used to determine the structure of Pt_xO_y ensemble. The chemical valence state of Pt for the fully oxidized Pt_xO_y was about + 1.30 (35 % Pt^0) according to the XPS analyses (Figs. 4c and 4 f). Firstly, we calculated the total Pt Bader charges of metal Pt and PtO, and the results are 0 and + 0.77 |e|, respectively. The structures of metal Pt and PtO slab used here were shown in Fig. S21, both with 96 atoms. The linear function relationship between Pt valence state and Bader charge was then established by setting Pt^0 and Pt^{2+} as the starting point and ending point, respectively (Fig. 5e). The valence state of + 1.30 will correspond to the Bader charge of + 0.50 |e| according to the function relationship. A series of $Pt_{10}O_y$, such as $Pt_{10}O_3$, $Pt_{10}O_5$ and $Pt_{10}O_8$, on CeO_2 were build and their relaxed structures are shown in Fig. 5f-h. As a result, $Pt_{10}O_8$-CeO_2 exactly exhibits an average Pt Bader charge of + 0.50 |e| (Fig. 5e) and the Bader charge of every individual Pt atom was shown in Fig. S22. So $Pt_{10}O_8$ is the representative structure of fully oxidized Pt_xO_y ensemble on CeO_2. In addition, the calculated forming energy of $Pt_{10}O_8$ is far lower than that of $Pt_{10}O_3$ and $Pt_{10}O_5$ on CeO_2 at 300 °C (Fig. S23), indicating its stability at the real reaction condition.

From the H_2-TPR results (Fig. 3a) and the conclusions of reference [57], it was deduced that the precursor species of Pt single atoms before reduction are oxidized Pt_1 or the aggregates of oxidized Pt_1. According to the analyses of CO-DRIFTS of the catalysts before reduction (Fig. 2b), the chemical valence state of oxidized Pt_1 should share similar value as PtO. We try to calculate Pt Bader charge of assumed oxidized Pt_1 structure to figure out one plausible precursor species of Pt single atom on CeO_2. Pt_1O_2 adsorbed at the step site of CeO_2 (named Pt_1O_2 @CeO_2-step, the structure was shown in Fig. 5i) was built by referring the work of Datye et al. [58]. Grunwaldt et al. [26] also reported a Pt^{2+}-O_2/CeO_2{110} DFT model with interfacial oxygen between the noble metal and CeO_2, which is similar to our model. The calculated

Bader charge of this Pt_1O_2 @CeO_2-step structure was + 0.72 |e|, which is close to the value of PtO (Fig. 5e). The adsorption properties of CO on different Pt sites of Pt_1O_2 @CeO_2-step and PtO surface were also explored. It can be found that CO desorbed from both surfaces after relaxations no matter which Pt site CO adsorbing (Fig. S24 and 25), suggesting CO is difficult to adsorb on the surface of fully oxidized Pt species, which is in line with the results of CO-DRIFTS shown in Fig. 2b. However, CO can adsorb on partly oxidized Pt species, such as Pt_xO_y ensemble, and the infrared spectra indicated that the vibrational frequency of CO adsorbed on it is similar to that of CO adsorbed on Pt single atom (Fig. 2a and Fig. 3c). The computational CO vibrational frequencies substantially support this viewpoint and the calculated frequencies upon Pt cluster and nanoparticle are also of great truthfulness (Table S4). The calculated energy barrier of CO oxidation on $Pt_{10}O_8$--CeO_2 (1.51 eV, Fig. S26) is larger than that of CO oxidation on defected Pt_4 and Pt_{10} on CeO_2 (Fig. S16 and 17), which is in consistent with the experimental results (Figs. 1d and 1 f).

In summary, the evolutions of Pt species on CeO_2 under certain atmospheres are significantly affected by the initial states of Pt. Fig. 6 shows the scheme of Pt species evolutions during H_2 reduction and CO oxidation. The oxidized Pt_1 at the step sites of CeO_2 under harsh reduction (300 °C) will migrate to the planar CeO_2 surface and some will aggregate to clusters (Fig. 6a), this phenomenon is similar to the view of Christopher et al. based on the analyses of Pt_{iso}/TiO_2 catalyst [57]. Whereas crystalline PtO will be reduced into Pt nanoparticles under the same condition (Fig. 6b). At the same time, CeO_2 surface oxygen vacancies are formed close to the Pt perimeter sites. Because of the different adsorption properties of CO and O_2 on Pt_1, Pt cluster and Pt nanoparticle, Pt species represent different behaviors of dynamics when being exposed in CO oxidation atmospheres. CO adsorbs on Pt_1 more strongly than O_2 (Fig. 5a), the charge state of Pt_1 will be changed by adsorbed CO, simultaneously, Pt_1 species become highly mobile with CO adsorption and thus aggregate to cluster by overcoming the diffusion barrier [71]. The similar adsorption energies for CO and O_2 on Pt clusters make Pt species dynamic stability during CO oxidation. However, O_2 adsorbs on Pt nanoparticle more strongly than CO, thus extra O will strongly bond to surface Pt atom except reacting with CO. Accordingly, Pt_xO_y ensembles are gradually formed with the elevated reaction temperatures more than 120 °C, and the coordinated O atoms will reach saturation at ~290 °C. The CO oxidation activity of Pt_xO_y ensemble seems among that of PtO and Pt_1 on CeO_2 (Fig. 1c and Fig. S1a).

4. Conclusions

A series of Pt-CeO_2 catalysts with Pt loading amounts ranged from 0.05 % to 0.75 % were fabricated by impregnation and calcination at 400 °C in air. It was found that the activities of these catalysts (after H_2 reductions) for CO oxidation are not in line with Pt loading amounts; the reactivity started to sharply decrease and the "hysteresis loop" in activity would appear when Pt loading amount is more than 0.25 %. These phenomena are closely related to the redox property of support and especially the surface structure of exposed facet. Surface lattice oxygen and the defective sites of CeO_2 were proved to play crucial role in both CO oxidation performance and the dynamic evolution of Pt state during reaction. Based on the analyses of reaction kinetics, chemisorption experiments and spectroscopic technology, it is concluded that Pt single atoms are prone to aggregate into Pt clusters while Pt nanoparticles suffer an oxidation process and gradually form a new Pt species-Pt_xO_y ensembles with the elevated reaction temperatures. The formation of Pt_xO_y ensemble and its poor reactivity substantially caused hysteresis in the light-off curve. DFT calculations further revealed that the different adsorption properties of CO and O_2 on Pt_1, Pt cluster and Pt nanoparticle are the primary causes of different evolution behaviors during CO oxidation for Pt species with different initial states. CO adsorbs on Pt_1 more strongly than O_2 while the situation was inversed for these adsorbates on Pt nanoparticle. The preferential bonding between CO/O_2 and Pt species caused Pt_1 sintering to small cluster and Pt nanoparticle being oxidized to Pt_xO_y ensemble in reaction atmospheres. Whereas the similar adsorption energies for CO and O_2 on Pt cluster make this Pt species dynamic stability during CO oxidation. At last, the representative structure of coordinating oxygen-saturated Pt_xO_y ensemble was figured out through Bader charge calculations based on the experimental valence analyses. Our study points out the importance of tracking reaction-driven dynamics of metal states in understanding the structure-performance relationship under real reaction conditions.

CRediT authorship contribution statement

Jinshi Dong: Supervision, Methodology, Writing – original draft. **Yutao Zhang:** Experiment, Formal analysis. **Dekun Li:** Experiment, Formal analysis. **Alexander Adogwa:** Writing – review & editing. **Shijun Huang:** Experiment. **Ming Yang:** Supervision. **Jiaqiang Yang:** Theoretical calculations. **Qianqian Jin:** Visualization.

Declaration of Competing Interest

The authors declare that they have no known competing financial interests or personal relationships that could have appeared to influence the work reported in this paper.

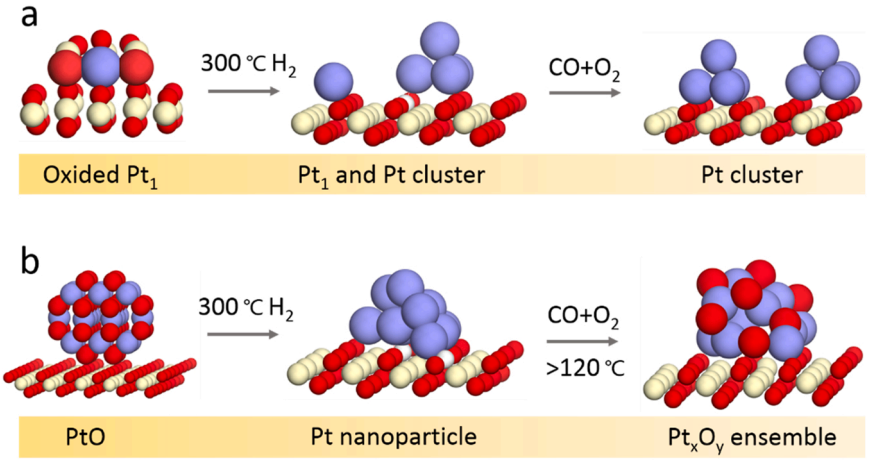

Fig. 6. Schematic overview of Pt species evolutions during H_2 reduction pretreatment and subsequent CO oxidation. (a) Oxidized Pt single atom on the surface of CeO_2. (b) PtO crystal on the surface of CeO_2. Color: Ce, yellow; O, red; Pt, purple; O_v, white.

Data availability

Data will be made available on request.

Acknowledgements

This work was financially supported by the National Natural Science Foundation of China (22162005), the Natural Science Foundation of Guangxi Province (2020GXNSFBA159013) and the Dr. Fund of GXUST (18Z14). We would also thank Liao from Shiyanjia Lab (www.shiyanjia.com) for the XPS tests.

Appendix A. Supporting information

Supplementary data associated with this article can be found in the online version at doi:10.1016/j.apcatb.2023.122662.

References

[1] F.C. Meunier, L. Cardenas, H. Kaper, B. Smid, M. Vorokhta, R. Grosjean, D. Aubert, K. Dembele, T. Lunkenbein, Synergy between metallic and oxidized Pt sites unravelled during room temperature CO oxidation on Pt/Ceria, Angew. Chem. Int Ed. Engl. 60 (2021) 3799–3805.
[2] B. Song, D. Choi, Y. Xin, C.R. Bowers, H. Hagelin-Weaver, Ultra-low loading Pt/CeO2 catalysts: ceria facet effect affords improved pairwise selectivity for parahydrogen enhanced NMR spectroscopy, Angew. Chem. Int. Ed. Engl., 60 (2021) 4038–4042.
[3] H. Jeong, D. Shin, B.S. Kim, J. Bae, S. Shin, C. Choe, J.W. Han, H. Lee, Controlling the oxidation state of Pt single atoms for maximizing catalytic activity, Angew. Chem. Int Ed. Engl. 59 (2020) 20691–20696.
[4] Q. Wang, Y. Li, A. Serrano-Lotina, W. Han, R. Portela, R. Wang, M.A. Banares, K. L. Yeung, Operando investigation of toluene oxidation over 1D Pt@CeO_2 derived from Pt cluster-containing MOF, J. Am. Chem. Soc. 143 (2021) 196–205.
[5] L. Zhang, Q. Bao, B. Zhang, Y. Zhang, S. Wan, S. Wang, J. Lin, H. Xiong, D. Mei, Y. Wang, Distinct role of surface hydroxyls in single-atom Pt_1/CeO_2 catalyst for room-temperature formaldehyde oxidation: acid-base versus redox, JACS Au 2 (2022) 1651–1660.
[6] H. Jeong, O. Kwon, B.-S. Kim, J. Bae, S. Shin, H.-E. Kim, J. Kim, H. Lee, Highly durable metal ensemble catalysts with full dispersion for automotive applications beyond single-atom catalysts, Nat. Catal. 3 (2020) 368–375.
[7] H. Xiong, D. Kunwar, D. Jiang, C.E. García-Vargas, H. Li, C. Du, G. Canning, X. I. Pereira-Hernandez, Q. Wan, S. Lin, S.C. Purdy, J.T. Miller, K. Leung, S.S. Chou, H. H. Brongersma, R. ter Veen, J. Huang, H. Guo, Y. Wang, A.K. Datye, Engineering catalyst supports to stabilize PdO_x two-dimensional rafts for water-tolerant methane oxidation, Nat. Catal. 4 (2021) 830–839.
[8] H. Xiong, S. Lin, J. Goetze, P. Pletcher, H. Guo, L. Kovarik, K. Artyushkova, B. M. Weckhuysen, A.K. Datye, Thermally stable and regenerable platinum-tin clusters for propane dehydrogenation prepared by atom trapping on ceria, Angew. Chem. 129 (2017) 9114–9119.
[9] F. Xing, Y. Nakaya, S. Yasumura, K.-i Shimizu, S. Furukawa, Ternary platinum–cobalt–indium nanoalloy on ceria as a highly efficient catalyst for the oxidative dehydrogenation of propane using CO_2, Nat. Catal.s 5 (2022) 55–65.
[10] L. Chen, P. Verma, K. Hou, Z. Qi, S. Zhang, Y.S. Liu, J. Guo, V. Stavila, M. D. Allendorf, L. Zheng, M. Salmeron, D. Prendergast, G.A. Somorjai, J. Su, Reversible dehydrogenation and rehydrogenation of cyclohexane and methylcyclohexane by single-site platinum catalyst, Nat. Commun. 13 (2022) 1092.
[11] L.N. Chen, K.P. Hou, Y.S. Liu, Z.Y. Qi, Q. Zheng, Y.H. Lu, J.Y. Chen, J.L. Chen, C. W. Pao, S.B. Wang, Y.B. Li, S.H. Xie, F.D. Liu, D. Prendergast, L.E. Klebanoff, V. Stavila, M.D. Allendorf, J. Guo, L.S. Zheng, J. Su, G.A. Somorjai, Efficient hydrogen production from methanol using a single-site Pt_1/CeO_2 catalyst, J. Am. Chem. Soc. 141 (2019) 17995–17999.
[12] S. Chen, S. Li, R. You, Z. Guo, F. Wang, G. Li, W. Yuan, B. Zhu, Y. Gao, Z. Zhang, H. Yang, Y. Wang, Elucidation of active sites for CH_4 catalytic oxidation over Pd/CeO_2 via tailoring metal–support interactions, ACS Catal. 11 (2021) 5666–5677.
[13] H. Ha, S. Yoon, K. An, H.Y. Kim, Catalytic CO oxidation over Au nanoparticles supported on CeO_2 nanocrystals: effect of the Au–CeO_2 interface, ACS Catal. 8 (2018) 11491–11501.
[14] J. Dong, D. Li, Y. Zhang, P. Chang, Q. Jin, Insights into the CeO_2 facet-depended performance of propane oxidation over Pt-CeO_2 catalysts, J. Catal. 407 (2022) 174–185.
[15] S. Xie, L. Liu, Y. Lu, C. Wang, S. Cao, W. Diao, J. Deng, W. Tan, L. Ma, S.N. Ehrlich, Y. Li, Y. Zhang, K. Ye, H. Xin, M. Flytzani-Stephanopoulos, F. Liu, Pt atomic single-layer catalyst embedded in defect-enriched ceria for efficient CO oxidation, J. Am. Chem. Soc. 144 (2022) 21255–21266.
[16] D. Jiang, G. Wan, C.E. García-Vargas, L. Li, X.I. Pereira-Hernández, C. Wang, Y. Wang, Elucidation of the active sites in single-atom Pd_1/CeO_2 CAtalysts for Low-temperature Co Oxidation, ACS Catal. 10 (2020) 11356–11364.
[17] J. Jones, H. Xiong, A.T. Delariva, E.J. Peterson, H. Pham, S.R. Challa, G. Qi, S. Oh, M.H. Wiebenga, X. Hernández, et al., Thermally stable single-atom platinum-on-ceria catalysts via atom trapping, Science 353 (2016) 150–154.
[18] L. Nie, D. Mei, H. Xiong, B. Peng, Z. Ren, X.I.P. Hernandez, A. DeLaRiva, M. Wang, M.H. Engelhard, L. Kovarik, A.K. Datye, Y. Wang, Activation of surface lattice oxygen in single-atom Pt/CeO_2 for low-temperature CO oxidation, Science 358 (2017) 1419–1423.
[19] A. Aitbekova, L. Wu, C.J. Wrasman, A. Boubnov, A.S. Hoffman, E.D. Goodman, S. R. Bare, M. Cargnello, Low-temperature restructuring of ceo2-supported ru nanoparticles determines selectivity in CO_2 catalytic reduction, J. Am. Chem. Soc. 140 (2018) 13736–13745.
[20] W. Huang, A.C. Johnston-Peck, T. Wolter, W.D. Yang, L. Xu, J. Oh, B.A. Reeves, C. Zhou, M.E. Holtz, A.A. Herzing, A.M. Lindenberg, M. Mavrikakis, M. Cargnello, Steam-created grain boundaries for methane C-H activation in palladium catalysts, Science 373 (2021) 1518–1523.
[21] H. Wang, J.X. Liu, L.F. Allard, S. Lee, J. Liu, H. Li, J. Wang, J. Wang, S.H. Oh, W. Li, M. Flytzani-Stephanopoulos, M. Shen, B.R. Goldsmith, M. Yang, Surpassing the single-atom catalytic activity limit through paired Pt-O-Pt ensemble built from isolated Pt_1 atoms, Nat. Commun. 10 (2019) 3808.
[22] L. Liu, D.M. Meira, R. Arenal, P. Concepcion, A.V. Puga, A. Corma, Determination of the evolution of heterogeneous single metal atoms and nanoclusters under reaction conditions: which are the working catalytic sites? ACS Catal. 9 (2019) 10626–10639.
[23] L. Song, H. Wang, S. Wang, Z. Qu, Dual-site activation of H_2 over Cu/$ZnAl_2O_4$ boosting CO_2 hydrogenation to methanol, Appl. Catal. B Environ. 322 (2023).
[24] W. Tan, S. Xie, D. Le, W. Diao, M. Wang, K.B. Low, D. Austin, S. Hong, F. Gao, L. Dong, L. Ma, S.N. Ehrlich, T.S. Rahman, F. Liu, Fine-tuned local coordination environment of Pt single atoms on ceria controls catalytic reactivity, Nat. Commun. 13 (2022) 7070.
[25] N. Daelman, M. Capdevila-Cortada, N. Lopez, Dynamic charge and oxidation state of Pt/CeO_2 single-atom catalysts, Nat. Mater. 18 (2019) 1215–1221.
[26] F. Maurer, J. Jelic, J. Wang, A. Gänzler, P. Dolcet, C. Wöll, Y. Wang, F. Studt, M. Casapu, J.-D. Grunwaldt, Tracking the formation, fate and consequence for catalytic activity of Pt single sites on CeO_2, Nat. Catal. 3 (2020) 824–833.
[27] V. Muravev, J.F.M. Simons, A. Parastaev, M.A. Verheijen, J.J.C. Struijs, N. Kosinov, E.J.M. Hensen, Operando spectroscopy unveils the catalytic role of different palladium oxidation states in CO oxidation on Pd/CeO_2 catalysts, Angew. Chem. Int Ed. Engl. 61 (2022), e202200434.
[28] G.S. Parkinson, Z. Novotny, G. Argentero, M. Schmid, J. Pavelec, R. Kosak, P. Blaha, U. Diebold, Carbon monoxide-induced adatom sintering in a Pd-Fe_3O_4 model catalyst, Nat. Mater. 12 (2013) 724–728.
[29] R. Bliem, J.E. van der Hoeven, J. Hulva, J. Pavelec, O. Gamba, P.E. de Jongh, M. Schmid, P. Blaha, U. Diebold, G.S. Parkinson, Dual role of CO in the stability of subnano Pt clusters at the Fe_3O_4(001) surface, Proc. Natl. Acad. Sci. USA 113 (2016) 8921–8926.
[30] X.I. Pereira-Hernandez, A. DeLaRiva, V. Muravev, D. Kunwar, H. Xiong, B. Sudduth, M. Engelhard, L. Kovarik, E.J.M. Hensen, Y. Wang, A.K. Datye, Tuning Pt-CeO_2 interactions by high-temperature vapor-phase synthesis for improved reducibility of lattice oxygen, Nat. Commun. 10 (2019) 1358.
[31] A.M. Gänzler, M. Casapu, F. Maurer, H. Störmer, D. Gerthsen, G. Ferré, P. Vernoux, B. Bornmann, R. Frahm, V. Murzin, M. Nachtegaal, M. Votsmeier, J.-D. Grunwaldt, Tuning the Pt/CeO_2 interface by in situ variation of the Pt particle size, ACS Catal. 8 (2018) 4800–4811.
[32] A.M. Ganzler, M. Casapu, P. Vernoux, S. Loridant, F.J. Cadete Santos Aires, T. Epicier, B. Betz, R. Hoyer, J.D. Grunwaldt, Tuning the structure of platinum particles on ceria in situ for enhancing the catalytic performance of exhaust gas catalysts, Angew. Chem. Int. Ed. Engl. 56 (2017) 13078–13082.
[33] V. Muravev, G. Spezzati, Y.-Q. Su, A. Parastaev, F.-K. Chiang, A. Longo, C. Escudero, N. Kosinov, E.J.M. Hensen, Interface dynamics of Pd–CeO_2 single-atom catalysts during CO oxidation, Nat. Catal. 4 (2021) 469–478.
[34] C. Dessal, T. Len, F. Morfin, J.-L. Rousset, M. Aouine, P. Afanasiev, L. Piccolo, Dynamics of single Pt atoms on alumina during CO oxidation monitored by operando X-ray and infrared spectroscopies, ACS Catal. 9 (2019) 5752–5759.
[35] C.P. O'Brien, G.R. Jenness, H. Dong, D.G. Vlachos, I.C. Lee, Deactivation of Pt/Al_2O_3 during propane oxidation at low temperatures: kinetic regimes and platinum oxide formation, J. Catal. 337 (2016) 122–132.
[36] Z. Cui, S. Song, H. Liu, Y. Zhang, F. Gao, T. Ding, Y. Tian, X. Fan, X. Li, Synergistic effect of Cu^+ single atoms and Cu nanoparticles supported on alumina boosting water-gas shift reaction, Appl. Catal. B Environ. 313 (2022).
[37] Z. Shao, S. Zhang, X. Liu, H. Luo, C. Huang, H. Zhou, Z. Wu, J. Li, H. Wang, Y. Sun, Maximizing the synergistic effect between Pt^0 and $Pt^{\delta+}$ in a confined Pt-based catalyst for durable hydrogen production, Appl. Catal. B Environ. 316 (2022).
[38] L. Kuai, Z. Chen, S. Liu, E. Kan, N. Yu, Y. Ren, C. Fang, X. Li, Y. Li, B. Geng, Titania supported synergistic palladium single atoms and nanoparticles for room temperature ketone and aldehydes hydrogenation, Nat. Commun. 11 (2020) 48.
[39] X. Zhang, M. Zhang, Y. Deng, M. Xu, L. Artiglia, W. Wen, R. Gao, B. Chen, S. Yao, X. Zhang, M. Peng, J. Yan, A. Li, Z. Jiang, X. Gao, S. Cao, C. Yang, A.J. Kropf, J. Shi, J. Xie, M. Bi, J.A. van Bokhoven, Y.W. Li, X. Wen, M. Flytzani-Stephanopoulos, C. Shi, W. Zhou, D. Ma, A stable low-temperature H(2)-production catalyst by crowding Pt on alpha-MoC, Nature 589 (2021) 396–401.
[40] W. Kohn, A.D. Becke, R.G. Parr, Density functional theory of electronic structure, J. Phys. Chem. 100 (1996) 12974–12980.
[41] G. Kresse, J. Hafner, Ab initio molecular dynamics for liquid metals, Phys. Rev. B 47 (1993) 558–561.

[42] G. Kresse, J. Hafner, Ab initio molecular-dynamics simulation of the liquid-metal–amorphous-semiconductor transition in germanium, Phys. Rev. B 49 (1994) 14251–14269.
[43] G.K. A, J.F. b, Efficiency of ab-initio total energy calculations for metals and semiconductors using a plane-wave basis set, Comput. Mater. Sci. 6 (1996) 15–50.
[44] G. Kresse, J. Furthmüller, Efficient iterative schemes for ab initio total-energy calculations using a plane-wave basis set, Phys. Rev. B 54 (1996) 11169–11186.
[45] J.P. Perdew, K. Burke, M. Ernzerhof, Generalized gradient approximation made simple, Phys. Rev. Lett. 77 (1996) 3865–3868.
[46] P.E. Blöchl, Projector augmented-wave method, Phys. Rev. B 50 (1994) 17953–17979.
[47] Q. Zhou, C. Zhou, Y. Zhou, W. Hong, S. Zou, X.-Q. Gong, J. Liu, L. Xiao, J. Fan, More than oxygen vacancies: a collective crystal-plane effect of CeO2 in gas-phase selective oxidation of benzyl alcohol, Catal. Sci. Technol. 9 (2019) 2960–2967.
[48] H.Y. Kim, H.M. Lee, G. Henkelman, CO oxidation mechanism on CeO_2-supported Au nanoparticles, J. Am. Chem. Soc. 134 (2012) 1560–1570.
[49] G. Henkelman, A. Arnaldsson, H. Jónsson, A fast and robust algorithm for Bader decomposition of charge density, Comput. Mater. Sci. 36 (2006) 354–360.
[50] H.V. Thang, G. Pacchioni, L. DeRita, P. Christopher, Nature of stable single atom Pt catalysts dispersed on anatase TiO_2, J. Catal. 367 (2018) 104–114.
[51] C. Dong, Z. Gao, Y. Li, M. Peng, M. Wang, Y. Xu, C. Li, M. Xu, Y. Deng, X. Qin, F. Huang, X. Wei, Y.-G. Wang, H. Liu, W. Zhou, D. Ma, Fully exposed palladium cluster catalysts enable hydrogen production from nitrogen heterocycles, Nat. Catal. 5 (2022) 485–493.
[52] J.L. Vincent, P.A. Crozier, Atomic level fluxional behavior and activity of CeO_2-supported Pt catalysts for CO oxidation, Nat. Commun. 12 (2021) 5789.
[53] S. Hinokuma, H. Fujii, M. Okamoto, K. Ikeue, M. Machida, Metallic Pd nanoparticles formed by Pd−O−Ce interaction: a reason for sintering-induced activation for CO oxidation, Chem. Mater. 22 (2010) 6183–6190.
[54] M.J. Kale, P. Christopher, Utilizing quantitative in situ FTIR spectroscopy to identify well-coordinated pt atoms as the active site for CO oxidation on Al_2O_3-supported Pt catalysts, ACS Catal. 6 (2016) 5599–5609.
[55] L. DeRita, S. Dai, K. Lopez-Zepeda, N. Pham, G.W. Graham, X. Pan, P. Christopher, Catalyst architecture for stable single atom dispersion enables site-specific spectroscopic and reactivity measurements of CO adsorbed to Pt atoms, oxidized Pt clusters, and metallic Pt clusters on TiO_2, J. Am. Chem. Soc. 139 (2017) 14150–14165.
[56] J. Ke, W. Zhu, Y. Jiang, R. Si, Y.-J. Wang, S.-C. Li, C. Jin, H. Liu, W.-G. Song, C.-H. Yan, Y.-W. Zhang, Strong local coordination structure effects on subnanometer PtO_x Clusters over CeO_2 nanowires probed by low-temperature CO oxidation, ACS Catal. 5 (2015) 5164–5173.
[57] L. DeRita, J. Resasco, S. Dai, A. Boubnov, H.V. Thang, A.S. Hoffman, I. Ro, G. W. Graham, S.R. Bare, G. Pacchioni, X. Pan, P. Christopher, Structural evolution of atomically dispersed Pt catalysts dictates reactivity, Nat. Mater. 18 (2019) 746–751.
[58] D. Kunwar, S. Zhou, A. DeLaRiva, E.J. Peterson, H. Xiong, X.I. Pereira-Hernández, S.C. Purdy, R. ter Veen, H.H. Brongersma, J.T. Miller, H. Hashiguchi, L. Kovarik, S. Lin, H. Guo, Y. Wang, A.K. Datye, Stabilizing high metal loadings of thermally stable platinum single atoms on an industrial catalyst support, ACS Catal. 9 (2019) 3978–3990.
[59] H. Daly, J. Ni, D. Thompsett, F.C. Meunier, On the usefulness of carbon isotopic exchange for the operando analysis of metal–carbonyl bands by IR over ceria-containing catalysts, J. Catal. 254 (2008) 238–243.
[60] A. Paredes-Nunez, I. Jbir, D. Bianchi, F.C. Meunier, Spectrum baseline artefacts and correction of gas-phase species signal during diffuse reflectance FT-IR analyses of catalysts at variable temperatures, Appl. Catal. A Gen. 495 (2015) 17–22.
[61] F.C. Meunier, Relevance of IR spectroscopy of adsorbed CO for the characterization of heterogeneous catalysts containing isolated atoms, J. Phys. Chem. C. 125 (2021) 21810–21823.
[62] X. Li, X.I. Pereira-Hernandez, Y. Chen, J. Xu, J. Zhao, C.W. Pao, C.Y. Fang, J. Zeng, Y. Wang, B.C. Gates, J. Liu, Functional CeO(x) nanoglues for robust atomically dispersed catalysts, Nature 611 (2022) 284–288.
[63] F.C. Meunier, T. Elgayyar, K. Dembélé, H. Kaper, Stability of Pt-adsorbed CO on catalysts for room temperature-oxidation of CO, Catalysts 12 (2022) 532.
[64] J.X. Liu, Y. Su, I.A.W. Filot, E.J.M. Hensen, A linear scaling relation for CO oxidation on CeO(2)-supported Pd, J. Am. Chem. Soc. 140 (2018) 4580–4587.
[65] M. Kottwitz, Y. Li, R.M. Palomino, Z. Liu, G. Wang, Q. Wu, J. Huang, J. Timoshenko, S.D. Senanayake, M. Balasubramanian, D. Lu, R.G. Nuzzo, A. I. Frenkel, Local structure and electronic state of atomically dispersed Pt supported on nanosized CeO2, ACS Catal. 9 (2019) 8738–8748.
[66] R. Kopelent, J.A. van Bokhoven, J. Szlachetko, J. Edebeli, C. Paun, M. Nachtegaal, O.V. Safonova, Catalytically active and spectator Ce(3+) in ceria-supported metal catalysts, Angew. Chem. Int. Ed. Engl. 54 (2015) 8728–8731.
[67] Y. Lykhach, S.M. Kozlov, T. Skala, A. Tovt, V. Stetsovych, N. Tsud, F. Dvorak, V. Johanek, A. Neitzel, J. Myslivecek, S. Fabris, V. Matolin, K.M. Neyman, J. Libuda, Counting electrons on supported nanoparticles, Nat. Mater. 15 (2016) 284–288.
[68] Y. Kim, G. Collinge, M.S. Lee, K. Khivantsev, S.J. Cho, V.A. Glezakou, R. Rousseau, J. Szanyi, J.H. Kwak, Surface density dependent catalytic activity of single palladium atoms supported on ceria, Angew. Chem. Int. Ed. Engl. 60 (2021) 22769–22775.
[69] R. Mi, D. Li, Z. Hu, R.T. Yang, Morphology effects of CeO_2 nanomaterials on the catalytic combustion of toluene: a combined kinetics and diffuse reflectance infrared Fourier transform spectroscopy study, ACS Catal. 11 (2021) 7876–7889.
[70] K. Ding, A. Gulec, A.M. Johnson, N.M. Schweitzer, G.D. Stucky, L.D. Marks, P. C. Stair, Identification of active sites in CO oxidation and water-gas shift over supported Pt catalysts, Science 350 (2015) 189–192.
[71] J.-C. Liu, Y. Tang, Y.-G. Wang, T. Zhang, J. Li, Theoretical understanding of the stability of single-atom catalysts, Natl. Sci. Rev. 5 (2018) 638–641.